The Electronic and Magnetic Properties of Cation Ordered $Sr_2Mn_{2.23}Cr_{0.77}As_2O_2$

Gaynor B. Lawrence [1,2], Eve J. Wildman [1], Gavin B. G. Stenning [3], Clemens Ritter [2], Francois Fauth [4] and Abbie C. Mclaughlin* [1]

[1] The Chemistry Department, University of Aberdeen, Meston Walk, Aberdeen, AB24 3UE, Scotland.

[2] Institut Laue-Langevin, 71 Avenue des Martyrs, 38000 Grenoble, France.

[3] ISIS, Science and Technology Facilities Council, Rutherford Appleton Laboratory, Didcot, OX11 0QX, UK.

[4] CELLS-ALBA Synchrotron, E-08290 Cerdanyola del Vallès, Barcelona, Spain

Abstract

Several different mechanisms of magnetoresistance (MR) have been observed in 1111 $LnMnAsO_{1-x}F_x$ oxypnictides (Ln = lanthanide) as a result of magnetic coupling between the Mn and Ln. Such phases also exhibit interesting magnetic phase transitions upon cooling. $Sr_2Mn_2CrAs_2O_2$ has been synthesised in order to investigate if it's possible to observe MR and/or magnetic phase transitions as a result of magnetic coupling between the Mn and Cr. $Sr_2Mn_2CrAs_2O_2$ crystallises with the *I*4/*mmm* tetragonal space group containing alternating MO_2^{2-} and $M'_2As_2^{2-}$ layers and neutron diffraction results demonstrate that the actual stoichiometry is $Sr_2Mn_{2.23}Cr_{0.77}As_2O_2$. Cation order is present between Mn and Cr, with Cr predominantly occupying the square planar MO_2^{2-} site. Below 410 K the magnetic moments of the Mn/Cr ions in the $M'_2As_2^{2-}$ sublattice exhibit G-type antiferromagnetic order. The Mn/Cr moments within the MO_2^{2-} layer order below 167 K with a K_2NiF_4-type-antiferromagnetic structure which simultaneously induces a spin-flip of the magnetic moments in the $M'_2As_2^{2-}$ layers from a G- to C-type antiferromagnetic arrangement. The results demonstrate that the

superexchange interactions are finely balanced in $Sr_2Mn_{2.23}Cr_{0.77}As_2O_2$. $Sr_2Mn_{2.23}Cr_{0.77}As_2O_2$ is semiconducting and there is no evidence of MR.

INTRODUCTION

Pnictide phases containing layers of *M*As (*M* = Fe, Mn) have been the subject of recent interest due to their potential as high temperature superconductors [1] and colossal magnetoresistant (CMR) materials [2]. Several iron-based pnictide systems exhibit superconductivity [3, 4], with the 1111-type, *Ln*FeAsO$_{1-x}$F$_x$ (*Ln*= La, Ce, Pr, Nd, Sm), displaying superconducting transition temperatures (T_c) of over 50 K [5]. In addition to the iron-based compounds, several pnictide materials containing MnAs layers have been shown to exhibit a wide array of interesting phenomena. NdMnAsO$_{1-x}$F$_x$ exhibits CMR of up to -95% between x = 0.05 - 0.08 [2, 6] . Replacing Nd with Pr to produce PrMnAsO$_{1-x}$F$_x$ showed remarkably different results. A large negative magnetoresistance was observed below 34 K [7] as a consequence of a structural tetragonal – orthorhombic transition driven by the Pr 4f electrons degrees of freedom. In contrast, a sizeable positive magnetoresistance appears in strontium doped Nd$_{1-x}$Sr$_x$MnAsO [8]; indicating that multiple mechanisms for MR are possible upon hole or electron doping the *Ln*MnAsO system (*Ln* = La, Pr, Nd).

Several layered pnictide phases $A_2M_3As_2O_2$ (*A* = Ba, Sr, M_3 = Mn_3, Cr_3, $MnZn_2$, Zn_3, Mn_2Cu) [9, 10, 11, 12, 13, 14, 15] have been synthesised. The unit cell contains alternating layers of square-planar MO_2 and *M'*As, similar to the CuO_2 layers in the high T_c cuprates and FeAs planes in the superconducting pnictide materials. It has been postulated that this unique structural relationship may deliver novel parent compounds for high temperature superconductivity, therefore further research into their structural, electronic and magnetic properties is warranted. Neutron diffraction and magnetic susceptibility measurements [15] revealed that $Sr_2Mn_3As_2O_2$ crystallises with a tetragonal unit cell with the space group *I*4/*mmm*, and no structural phase transitions were detected down to 4 K. The structure contains layers of MnO_2^{2-} (Mn(1)) and $Mn_2As_2^{2-}$ (Mn(2)) blocks, alternating along the *c* axis of the unit cell, separated by Sr layers. The Mn(2) sublattice demonstrates long range AFM order below T_N = 340 K, with moments aligned parallel to the *c* axis with a G-type antiferromagnetic structure and a saturated moment of 3.4 μ_B, similar to $BaMn_2As_2$ [16]. A second magnetic transition occurs below 75 K, associated with Mn(1) moments within the MnO_2 layer. The weak magnetic reflections which

have been tentatively indexed with k = [½ ½ 0] exhibit a Warren lineshape, indicative of two-dimensional magnetism. Resistivity data, ρ(T), revealed that $Sr_2Mn_3As_2O_2$ is a narrow band gap semiconductor with an activation energy of 147(5) meV. Introducing Zn into the structure produces the phase, $Sr_2Zn_2MnAs_2O_2$ [17]. Zn occupies the $M'_2As_2^{2-}$ blocks and the compound is also a semiconductor, with spin-glass type behaviour. $Sr_2Mn_2CuAs_2O_2$ has also been synthesised, where Cu replaces some of the Mn in the $M'_2As_2^{2-}$ layers and is a ferrimagnetic metal [9].

$Sr_2Cr_3As_2O_2$ has recently been synthesised [11, 12], and is isostructural with $Sr_2Mn_3As_2O_2$; containing $Cr_2As_2^{2-}$ and CrO_2^{2-} layers. Two magnetic transitions occur below 590 K and 291 K, associated with the $Cr_2As_2^{2-}$ and CrO_2^{2-} layers respectively. Below 590 K the Cr ions in the Cr_2As_2 sublattice order in a C-type antiferromagnetic arrangement with spins aligned parallel to *c*. Below 291 K the Cr ions within the CrO_2 sublattice order with a K_2NiF_4-like magnetic structure with *c* as the easy axis. At the same time a spin-flip transition occurs within the $Cr_2As_2^{2-}$ sublattice, the moment direction rotates from the *c* axis to the *ab* plane. $Sr_2Cr_3As_2O_2$ is metallic, similar to $BaCr_2As_2$ [18] and LaCrAsO [19]. In this paper we describe the electronic properties, crystal and magnetic structure of the new phase $Sr_2Mn_2CrAs_2O_2$. The stoichiometry $Sr_2Mn_2CrAs_2O_2$ was targeted to see if it was possible to obtain a phase with ordered $Mn_2As_2^{2-}$ and CrO_2^{2-} layers which could exhibit interesting MR and/or magnetic phase transitions as a result of magnetic coupling between the Mn and Cr. This new phase displays two magnetic transitions at ~ 167 K and 410 K, associated with magnetic order within the MO_2^{2-} and $M'_2As_2^{2-}$ layers respectively (M = Mn/Cr). Below 167 K there is a magnetic rearrangement in the $M'_2As_2^{2-}$ layers from G- to C-type antiferromagnetism with spins remaining aligned parallel to *c*. In contrast when the Cr spins order in the CrO_2^{2-} plane in $Sr_2Cr_3As_2O_2$ the moments in the $Cr_2As_2^{2-}$ layers, which exhibit C-type antiferromagnetism, reorient from the *c* axis to the *ab* plane. The spins in the $Mn_2As_2^{2-}$ layers remain G-type down to base temperature in $Sr_2Mn_3As_2O_2$.

EXPERIMENTAL

A polycrystalline sample of $Sr_2Mn_2CrAs_2O_2$ was prepared by the solid-state reaction of the starting materials SrO (99.99% Aldrich), Mn (99.98% Aldrich), Cr (99.98% Aldrich) and As pieces (99.97% Alfa Aesar). SrO was prepared by heating $SrCO_3$ (99.99% Aldrich) at 1200°C for 12h and the de-carbonated material was subsequently cooled under vacuum. Stoichiometric amounts of Mn, Cr and As were mixed with non-stoichiometric amounts of SrO with a 2% wt. deficiency. This small oxygen deficiency was necessary in order to increase phase purity, similar to the reported synthesis for $Sr_2Cr_3As_2O_2$ [11]. The starting materials were ground together in an inert atmosphere using an agate pestle and mortar, pelleted and placed in an evacuated quartz tube which was heated at 800°C for 10h followed by an additional heating at 980°C for 48 hours. The sample was then reground and heated at 1000 °C for a further 48 hours.

A room temperature powder X-ray diffraction pattern of $Sr_2Mn_2CrAs_2O_2$ was collected using a PANalytical Empyrean Powder diffractometer with Cu $K_{\alpha 1}$ radiation. Data were recorded in the range $5° < 2\theta < 100°$, with a step size of 0.0131°. Variable temperature neutron diffraction patterns in the temperature range of 1.5 to 300 K were recorded on the high-resolution powder diffractometer D2B at the Institut Laue-Langevin (ILL) in Grenoble, France. Diffraction patterns were also recorded upon cooling on the D2B diffractometer between 200 and 120 K. A sample of 2 grams of $Sr_2Mn_2CrAs_2O_2$ was inserted in an 8 mm vanadium can and heated/cooled to the desired temperatures. Data were collected with $\lambda = 1.594$ Å with a total collection time of two hours for each temperature step. Neutron diffraction data were also collected on the high intensity D1B diffractometer at the ILL on the same sample. Data were recorded with $\lambda = 2.52$ Å from 3 - 446 K on heating. Neutron diffraction data were also collected upon cooling from 300 to 1.5 K, on the high intensity D20 diffractometer at the ILL with $\lambda = 2.42185$ Å. Both D20 and D1B data were recorded with a ramping rate of 19 seconds per 0.1°.

Synchrotron X-ray diffraction patterns were collected using a 0.4123 Å wavelength on the powder diffraction station on the BL04-MSPD beamline of the ALBA synchrotron in Barcelona, Spain [20].

The highest angular resolution was obtained using the so called Multi Analyzer Detection (MAD) setup. Powder diffraction patterns were collected in the angular range 0-45° 2θ with a step size of 0.003°. Low temperatures were achieved using the lHe flow cryostat Dynaflow [21] and data were recorded at 220 K, 180K, 155K, 120 K and 10K.

Magnetisation measurements of $Sr_2Mn_2CrAs_2O_2$ were recorded on a Quantum Design SQUID magnetometer in an applied field of 1000 Oe after zero field cooling (ZFC) and field cooling (FC) the sample at temperatures between 4 – 400 K.

The temperature dependence of the electrical resistance of $Sr_2Mn_2CrAs_2O_2$ was measured using a Quantum Design physical property measurement system (PPMS) between 4 and 400 K in fields of 0T and 7 T.

RESULTS AND DISCUSSION

The laboratory powder X-ray diffraction pattern of $Sr_2Mn_2CrAs_2O_2$ could be indexed on a tetragonal unit cell of space group *I*4/*mmm*, with unit cell parameters of a = 4.1061(1) Å and c = 19.0490(3) Å. A small impurity which could be indexed as $Cr_{0.7}Mn_{0.3}As$ (~ 5%) was also detected (Figure S1). The crystal structure of $Sr_2Mn_2CrAs_2O_2$ is displayed in Figure 1.

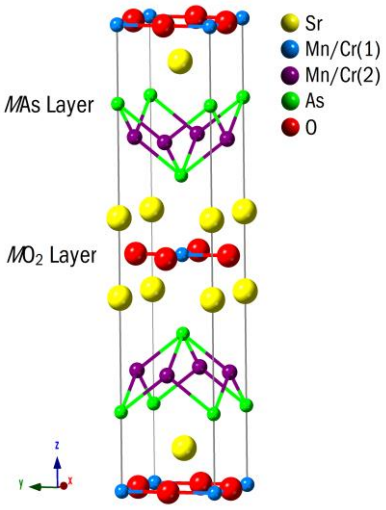

Figure 1 Crystal structure of $Sr_2Mn_2CrAs_2O_2$ showing the alternating M(1) CuO_2-type and M(2) FeAs-type layers along *c*.

The unit cell of $Sr_2M_3As_2O_2$ contains two distinct *M* sites, the 2*a* site located within the $M(1)O_2^{2-}$ planes and the 4*d* site which is contained within $M(2)_2As_2^{2-}$ layers. In order to determine the distribution of the two metal cations over the two distinct *M* sites in $Sr_2Mn_2CrAs_2O_2$, Rietveld refinement [22] was performed on the high-resolution neutron diffraction data between 1.5 K and 300 K using the FullProf Suite package [23]. Background points were selected from the baseline of the datafile, between the peaks and then refined. The peak shapes were fitted using a Pseudo-Voigt function. An excellent fit to the tetragonal *I*4/*mmm* symmetry space group was obtained at all temperatures. Figure 2 shows the Rietveld fits at 1.5 K and 300 K (a = 4.0935(1) Å, c = 19.0646(6) Å; χ^2 = 2.25, R_{WP} = 11.1% at 300 K; a = 4.08327(6) Å, c = 18.9936(3) Å; χ^2 = 3.14, R_{WP} = 12.3% at 1.5 K). Refined cell parameters, agreement factors and atomic parameters for $Sr_2Mn_2CrAs_2O_2$ at the different temperatures are displayed in Table S1. The strontium, oxygen and arsenic fractional occupancies refined to within ±1 % of the full occupancy and thus were fixed in further refinement at 1.0. The results from Rietveld refinement demonstrated that the Mn predominantly occupies the *M*(2) site (refined occupancy = 96%) and that the *M*(1) site is occupied by 68% Cr and 32% by Mn so that the refined stoichiometry is $Sr_2Mn_{2.23}Cr_{0.77}As_2O_2$ and will be referred to as such for the rest of the paper. It is likely that the non-stoichiometry arises due reaction of Cr with the silica tube. The mixed site occupancy at the *M*(1) site results in a small scattering length at this position as a result of the neutron scattering lengths of Mn (-3.73 fm) and Cr (3.635 fm). The isotropic atomic displacement parameters (B_{iso}) for the two *M* positions were therefore constrained to the same value. The impurity phase $Cr_{0.7}Mn_{0.3}As$ was included in the fit. The results demonstrate that there is cation order between Mn and Cr, so that Cr is predominantly found at the square planar *M*(1) site. This is attributed to the presence of the Jahn-Teller distortion and crystal field stabilisation energy (CFSE) of the d^4 electron configuration. Cr is predominantly found in either distorted octahedral or square planar geometry [24]. In contrast Mn is a high-spin d^5 system with no CFSE and will therefore occupy either position with no preference.

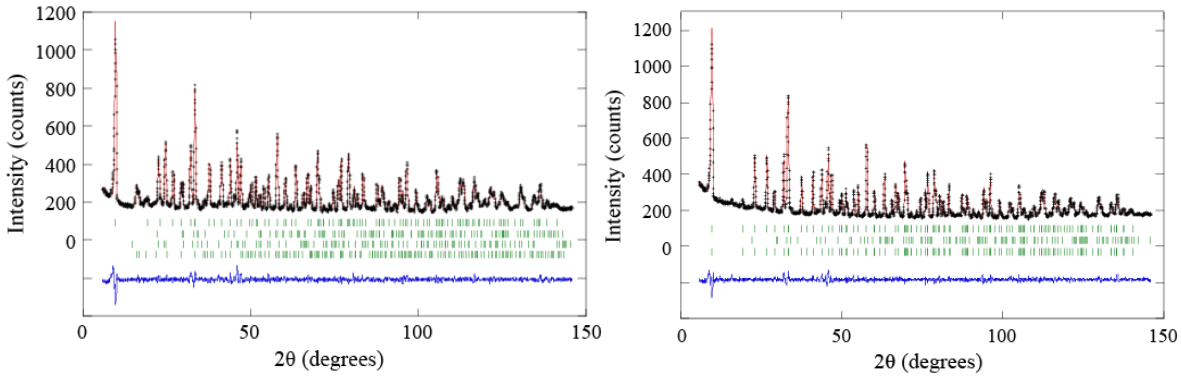

Figure 2 The Rietveld refinement fits to the *I*4/*mmm* structural model of $Sr_2Mn_{2.23}Cr_{0.77}As_2O_2$ at 1.5 K (left) and 300 K (right) (recorded upon heating). The secondary phase $Cr_{0.7}Mn_{0.3}As$ is included in the fit. Tick marks represent reflection positions for $Sr_2Mn_{2.23}Cr_{0.77}As_2O_2$, $Cr_{0.7}Mn_{0.3}As$ and the magnetic phase(s) from top to bottom respectively.

The high intensity neutron diffraction data, recorded between 1.5 K and 450 K, were used to follow the evolution of the neutron diffraction peaks with temperature (Fig. 3). Below 410 K the intensity of the (101) and (103) diffraction peaks are enhanced significantly suggesting a $k_1 = 0$ propagation vector, as no new reflections appear. The program BasiIreps, which is part of the FullProf Suite of programs, was used for symmetry analysis and the determination of the allowed magnetic structures. [23] The magnetic structure was refined with a G-type antiferromagnetic ordering of the Mn/Cr(2) spins with spins aligned parallel to *c* and an excellent fit of the high resolution data taken at 300 K was obtained (Figure 2, right) to this model. In this model the spins are aligned antiferromagnetically in all three crystallographic directions. The same magnetic structure has been reported for $Sr_2Mn_3As_2O_2$ and will be referred to as AFM-HT from now on (Figure 4).

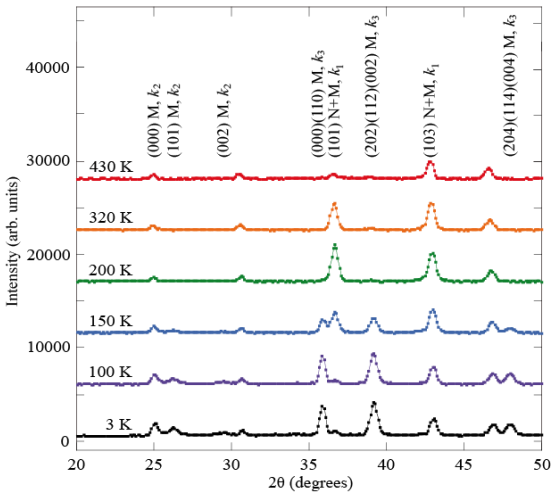

Figure 3 Selected high intensity neutron diffraction patterns recorded upon varying the temperature from 3 K – 430 K showing the evolution and appearance of the magnetic neutron diffraction peaks.

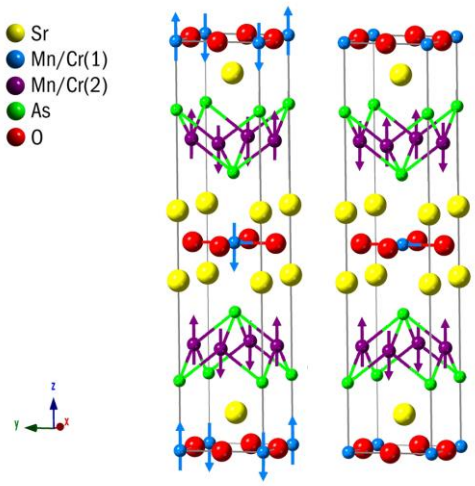

Figure 4 The magnetic structures of $Sr_2Mn_{2.23}Cr_{0.77}As_2O_2$ below 135 K (AFM-LT, left) and above 167 K (AFM-HT, right).

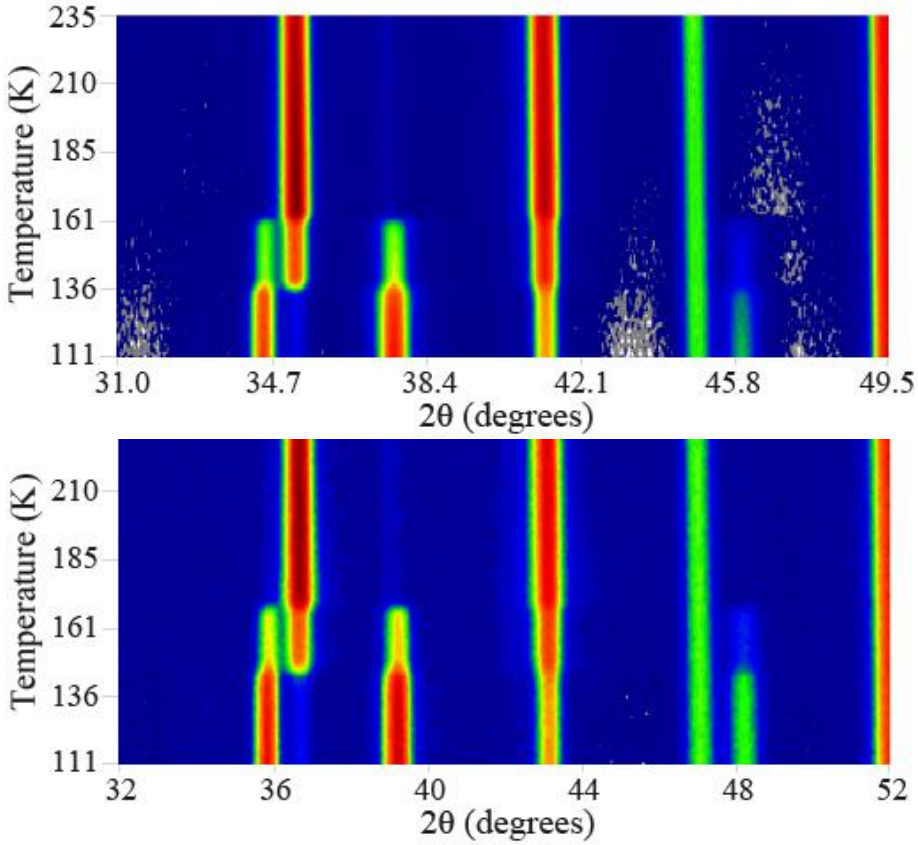

Figure 5 Contour plot from D1B (data recorded upon heating, top) and D20 (data recorded upon cooling, bottom) neutron diffraction data showing the peak intensities of a select 2θ region with varying temperature. Magnetic phase separation is clearly evidenced. Due to the different wavelengths of D1B and D20 the 2Θ positions of identical Bragg reflections are slightly shifted.

Below 167 K, new magnetic diffraction peaks appear (Figure 3) that are assigned to an AFM arrangement of the Mn/Cr (1) spins along *c* with a propagation vector k_2 = (½, ½, 0). This is the same magnetic structure as reported for $Sr_2Cr_3As_2O_2$ [12], with the *M*(1) moments ordering with the K_2NiF_4-type antiferromagnetic structure [25]. Simultaneously with the appearance of the *M*(1) magnetic order, further new magnetic diffraction peaks were detected. These extra peaks can be indexed by the propagation vector k_3 = (1, 0, 0) describing a C-type antiferromagnetic arrangement of the *M*(2) sites within the $M'_2As_2^{2-}$ sublattice with the moment direction along the *c* axis (Figures 3 and 4, left). In this antiferromagnetic structure the spins are aligned antiferromagnetically in the *ab* plane and

ferromagnetically along *c*. The same antiferromagnetic structure has been reported for $Sr_2Cr_3As_2O_2$ between 291 and 590 K[12]. However in $Sr_2Cr_3As_2O_2$ the ordering of the Cr(1) ions results in a concomitant spin flip of the magnetically ordered Cr(2) ions from the *c* axis direction into the *ab* plane. On the contrary, in $Sr_2Mn_{2.23}Cr_{0.77}As_2O_2$ the spins of the *M*(2) site flip from a G-type (k_1 = 0) to a C-type k_3 = (1, 0, 0) antiferromagnetic structure with the spins remaining parallel to *c*. At base temperature (1.5 K) the refined magnetic moments of *M*(1) and *M*(2) (Figure 6, left) are 3.94(6) μ_B/*M* and 3.38(2) μ_B/*M* for *M*(1) and *M*(2) respectively. For simplicity, the low temperature (< 167 K) magnetic structure is called AFM-LT (Figure 4, left). The $\sqrt{2}a$ x $\sqrt{2}a$ x *c* antiferromagnetic cell is also shown in Supplementary Figure S3.

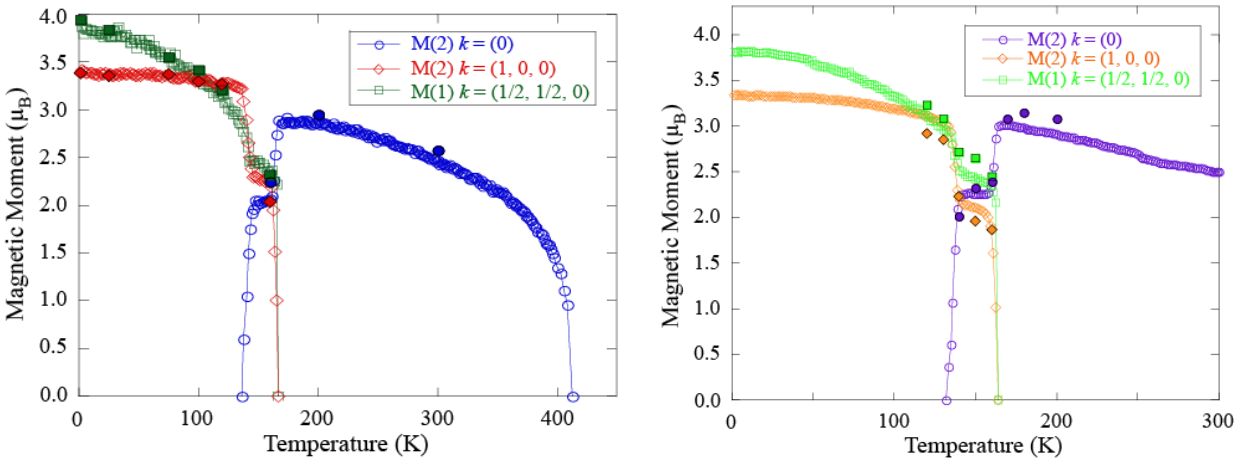

Figure 6 Variation of *M*(1) and *M*(2) magnetic moments with temperature from D1B (heating, left) and D20 (cooling, right) neutron diffraction data refinements. The filled points are from D2B neutron diffraction data refinements.

Surprisingly in the temperature region of 135 K - 167 K magnetic phase separation between the two antiferromagnetic structures displayed in Figure 4 is evidenced. A contour plot evidencing the magnetic phase separation between the two antiferromagnetic structures is shown in Figure 5. The (101) nuclear and magnetic peak at 36.8° arises from the G-type antiferromagnetic arrangement of the *M*(2) ions having k_1 = 0. The (000) and (202) magnetic peaks shown in Figure 5 at 35.5° and 39° correspond to the k_3 = (1,0,0) C-type antiferromagnetic arrangement of the same *M*(2) cations within the $M'_2As_2^{2-}$ layers. It is apparent that both antiferromagnetic structures are observed between ~ 135

K and 167 K. The magnetic peaks arising from the antiferromagnetic order of the M(1) site following k_2 = [½ ½ 0] behave similar to those of the k_3 phase. There is a slight hysteresis in the magnetic phase transition temperatures upon heating and cooling; the magnetic phase separation occurs between 138 K -167 K upon heating and 164 K – 135 K upon cooling (Figure 6).

The variation of the *M*(1) and *M*(2) magnetic moments refined from the high intensity D1B and D20 neutron diffraction data is displayed in Figure 6, the refined *M*(1) and *M*(2) moments from the high resolution D2B neutron diffraction data are also included as the solid symbols. Upon cooling, the magnetic moments of Mn/Cr ions on the *M*(2) site with $k_1 = 0$ increase to ~ 3 μ_B/M ion at 164 K. In the phase separation region, it was not possible to refine the scale factors of the magnetic structures and the magnetic moments simultaneously. Hence during refinement, the scale factors for the magnetic phases were constrained to be the same as the nuclear phase. It therefore appears in Figure 6 as if the magnetic moments on the *M*(1) and *M*(2) sites are reduced within the magnetic phase separation region. However, this is an artefact of the Rietveld refinement procedure and represents the reduced phase fraction of the two magnetic structures. If the phase fractions are refined, rather than the magnetic moments (and the magnetic moment of the *M*(2) site having the AFM-HT magnetic order is kept constant at its value adopted at the temperature just above the phase separation), the phase fractions of the two magnetic structures are 59.8% (AFM-HT) and 40.2% (AFM-LT) at 160 K upon cooling and 56.0% (AFM-HT) and 44.0% (AFM-LT) at 160 K upon heating. Between 167 K-146 K there is very little change in the magnitude of the moments on the *M*(1) or *M*(2) site or the phase fractions. The phase fraction of the AFM-HT magnetic structure decreases rapidly below 146 K and is no longer observed by 135 K. At the same time the phase fraction of the AFM-LT increases and is the only magnetic structure observed below 135 K.

The *a* and *c* cell parameters are displayed in Figure 7, where a subtle deviation from usual thermal expansion is observed at ~ 150 K so it appears that the magnetic behaviour is coupled to the lattice. Selected bond lengths and angles from Rietveld refinement are shown in Figure 8 and Table 1. The Sr-O, Sr-As, *M*(1)-As, *M*(2)-As and *M*(1)-O bond lengths all increase upon heating. The *M*(2)-As-

M(2) bond angle initially decreases from 69.05(3) ° to 68.97(3) ° upon raising the temperature before increasing above 150 K. Similar trends are observed for the As-*M*(2)-As bond angles (Table 1) indicating that the magnetic transitions influences the distortion of the tetrahedra within the $M'_2As_2^{2-}$ layer at 150 K, resulting in a subtle change in the *a* and *c* cell parameters.

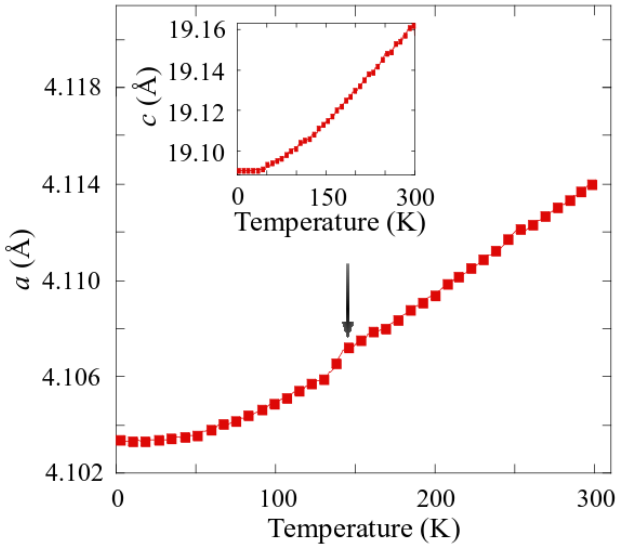

Figure 7 Temperature variation of *a* and *c* (inset) cell parameters upon heating. The magnetic transition is manifest in the *a* cell parameter as shown by the arrow.

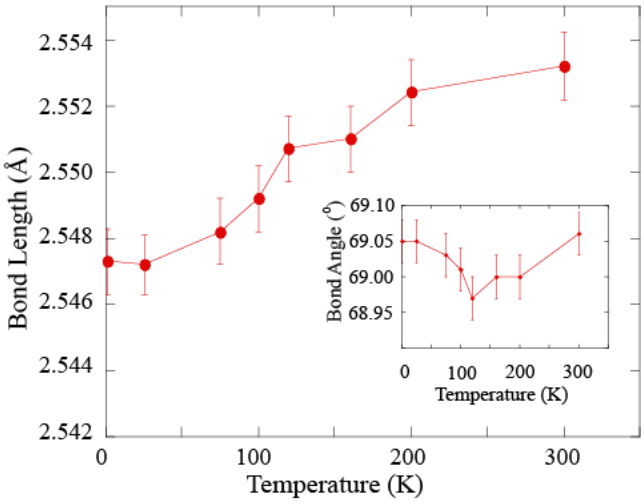

Figure 8 Temperature variation of *M*(2)-As bond length and *M*(2)-As-*M*(2) bond angle (inset).

Table 1 Temperature variation of selected bond lengths and angles from Rietveld fits against D2B neutron diffraction data recorded upon heating from 1.5 K – 300 K.

	Temperature (K)							
	1.5	25	75	100	120	160	200	300
Sr-As(Å)	3.2999(12)	3.3005(11)	3.2996(12)	3.3005(12)	3.2991(12)	3.3010(12)	3.3042(12)	3.3117(12)
Sr-O (Å)	2.6109(11)	2.6106(11)	2.6121(11)	2.6118(11)	2.6134(11)	2.6160(11)	2.6155(11)	2.6170(11)
Sr-M1 (Å)	3.3143(8)	3.3142(8)	3.3155(8)	3.3155(8)	3.3169(8)	3.3195(9)	3.3198(8)	3.3223(8)
Sr-M2 (Å)	3.7295(14)	3.7301(14)	3.7294(14)	3.7315(14)	3.7305(14)	3.7315(14)	3.7363(14)	3.7443(14)
M1-As (Å)	3.2251(17)	3.2256(15)	3.2252(17)	3.2254(17)	3.2241(17)	3.2283(17)	3.2304(17)	3.2298(17)
M1-O (Å)	2.04163(3)	2.04171(3)	2.04197(3)	2.04228(3)	2.04251(3)	2.04352(3)	2.04453(6)	2.04677(5)
M2-As (Å)	2.5473(10)	2.5472(9)	2.5482(10)	2.5492(10)	2.5507(10)	2.5510(10)	2.5524(10)	2.5532(10)
M2-M2 (Å)	2.88731(3)	2.88741(3)	2.88779(3)	2.88821(3)	2.88854(3)	2.88997(3)	2.89140(6)	2.89457(5)
M2-As-M2 (°)	69.05(3)	69.05(3)	69.03(3)	69.01(3)	68.97(3)	69.00(3)	69.00(3)	69.06(3)
As-M2-As 1 (°)	106.55(3)	106.56(3)	106.51(3)	106.48(3)	106.41(3)	106.46(3)	106.45(3)	106.57(3)
As-M2-As 2 (°)	110.95(7)	110.95(6)	110.97(7)	110.99(7)	111.03(7)	111.00(7)	111.00(7)	110.94(7)

Magnetic phase separation has been well studied in transition metal oxides such as the perovskite $La_{1-x}Ca_xMnO_3$ [26] and more recently in the ruthenate $Ca_3(Ru_{1-x}Ti_x)_2O_7$ [27] and the ferrite $CaFe_3O_5$ [28]. Electronic phase separation into antiferromagnetic and superconducting/normal state regions has been observed in Fe pnictides such as $Ba_{1-x}K_xFe_2As_2$ [29]. To investigate the observed magnetic phase separation in $Sr_2Mn_{2.23}Cr_{0.77}As_2O_2$ further, synchrotron X-ray diffraction data were recorded on the MSPD beamline of the ALBA synchrotron facility at selected temperatures between 10 K and 220 K. At all temperatures, a subtle splitting of the peaks is observed, evidencing that two phases are present within the sample. An excellent Rietveld fit to the two-phase model was obtained at all temperatures (Figures S4 and S5, Table S2 and S3). Both phases crystallise in the *I4/mmm* symmetry space group but have slightly different cell parameters (at 220 K a = 4.09082(2) Å, c = 19.0785(1) Å (phase 1); a = 4.09884(2) Å, c = 19.0288(1) Å (phase 2)). From the refinement results 60.8(4)% of the sample consists of phase 1 and 39.2(4)% is phase 2). The 300 K cell parameters of $Sr_2Mn_3As_2O_2$, $Sr_2Mn_{2.23}Cr_{0.77}As_2O_2$ and $Sr_2Cr_3As_2O_2$ are a = 4.22679(5) Å and c = 20.159(3) Å [15], a = 4.09354(10) Å and c = 19.0646(6) Å (from the neutron data) and a = 4.00671(6) Å and c = 18.8310(3) Å [11, 12] respectively. This would suggest that the two phases observed in the synchrotron diffraction data have slightly different Mn:Cr stoichiometry. Upon reinspection of the neutron diffraction data, it was possible to see very subtle broadening effects in the neutron data for some of the (h00) or (00l) reflections. However, it was not possible to fit the data to determine the exact stoichiometries of the phases. The segregation of the sample into two distinct phases explains the magnetic phase segregation shown in Figures 5 and 6. The phase fractions of the two magnetic phases refined to 59.8% (AFM-HT) and 40.2% (AFM-LT) at 160 K which agrees with the phase fractions obtained from the synchrotron X-ray diffraction data. This would suggest that phase 2 orders antiferromagnetically within the $M(1)O_2^{2-}$ planes at 167 K and phase 1 orders antiferromagnetically within the $M(1)O_2^{2-}$ plane at 135 K. The magnetic ordering temperature within the $M(1)O_2^{2-}$ plane

would appear to be very sensitive to small changes in stoichiometry with the phase containing the higher concentration of Cr in the $M(1)O_2^{2-}$ plane most likely ordering at 167 K.

The superexchange interactions would therefore appear to be very delicately balanced in the $Sr_2M_3As_2O_2$ phases [9, 11, 12, 14, 15]. In $Sr_2Mn_{3-x}Cr_xAs_2O_2$ the magnetic coupling between the $M(1)O_2^{2-}$ planes and the $M(2)_2As_2^{2-}$ slabs gets stronger as the Cr concentration increases from x = 0 - 3 so that the antiferromagnetic ordering temperatures increase from 0 K – 340 K ($M(1)O_2^{2-}$ plane (2D ordering is observed below 65 K for x = 0)) and 340 K - 530 K ($M(2)_2As_2^{2-}$ slabs). $Sr_2Mn_3As_2O_2$ and $Sr_2Mn_{2.23}Cr_{0.77}As_2O_2$ have practically the same chemical stoichiometry within the $Mn_2As_2^{2-}$ block but changes in the stoichiometry of the $M(1)O_2^{2-}$ plane from MnO_2^{2-} to $Cr_{0.68}Mn_{0.32}O_2^{2-}$ result in a substantial increase in the antiferromagnetic ordering temperatures from 0 K – 167 K ($M(1)O_2^{2-}$ plane and 340 K - 410 K ($M(2)_2As_2^{2-}$ slabs). It's been previously reported in the $Sr_2M_3As_2O_2$ phases that there is an increasing level of ferromagnetic correlations as the *c* axis and interlayer separation decrease [9]. In $Sr_2Cr_3As_2O_2$ the spins are aligned ferromagnetically along *c*. In contrast $Sr_2Mn_3As_2O_2$, which has a larger unit cell, exhibits G-type antiferromagnetic order within the $Mn_2As_2^{2-}$ block and doesn't exhibit 3-dimensional antiferromagnetic order within the MnO_2^{2-} as a result of magnetic frustration. The substitution of 68 % Cr onto the MnO_2^{2-} plane and subsequent decrease in cell parameters enhances the ferromagnetic correlations along *c*. This relieves the magnetic frustration so that the K_2NiF_4-type antiferromagnetic order is observed at elevated temperatures in the $Cr_{0.68}Mn_{0.32}O_2^{2-}$ plane and induces the simultaneous spin-flip of the Mn/Cr moments within the arsenide layers from a G-type to a C-type antiferromagnetic arrangement.

The temperature dependence of the magnetic susceptibility, for $Sr_2Mn_{2.23}Cr_{0.77}As_2O_2$ is shown in Figure 9. Two magnetic transitions are apparent. The broad transition at ~ 150 K corresponds to the AFM order of the *M*(1) moments and simultaneous spin flip of the magnetically ordered *M*(2) ions from the *c* axis direction into the *ab* plane. The 50 K transition is not observable in the neutron data which suggests it is due to the minor impurity in the sample. The magnetic susceptibility data show

a bifurcation of the FC and ZFC data at around 200 K which most likely arises from tiny quantities of ferromagnetic or spin-glassy impurities.

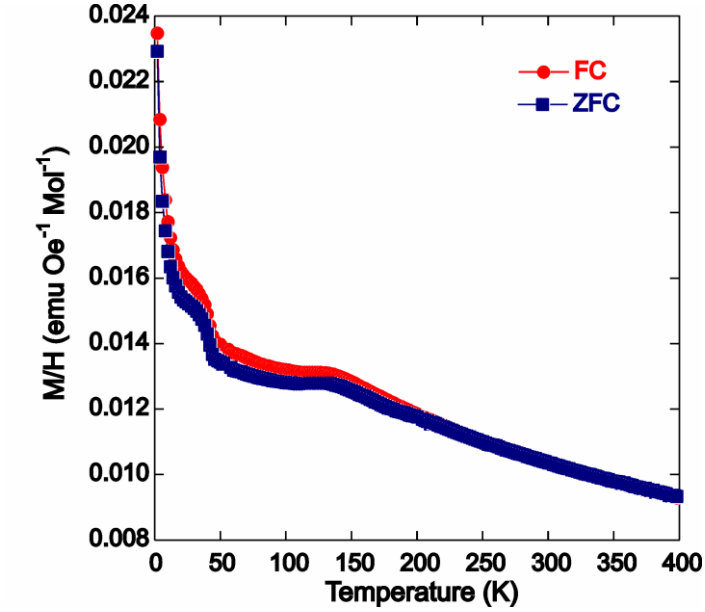

Figure 9 The temperature variation of the field cooled (FC) and zero field cooled (ZFC) susceptibility of $Sr_2Mn_{2.23}Cr_{0.77}As_2O_2$.

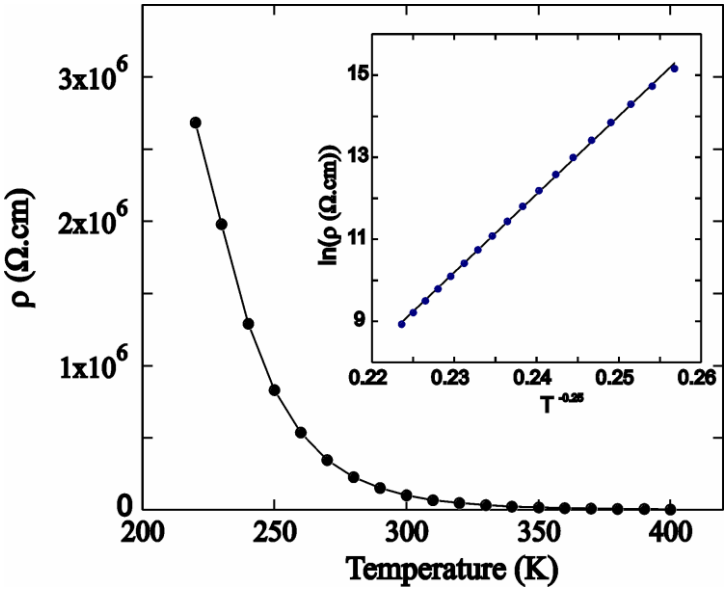

Figure 10 Temperature dependence of the electrical resistivity for the $Sr_2Mn_{2.23}Cr_{0.77}As_2O_2$ polycrystalline pellet. The inset shows the fit to the Mott three-dimensional variable range hopping equation.

The thermal variation of the electrical resistivity is displayed in Figure 10 which indicates that $Sr_2Mn_{2.23}Cr_{0.77}As_2O_2$ is a semiconductor. $Sr_2Mn_{2.23}Cr_{0.77}As_2O_2$ is too resistive to be measured below 210 K. There was no evidence of magnetoresistance in the temperature range measured. Above 210 K the electron transport could be modelled by Mott three-dimensional variable range hopping (3D VRH) of the charge carriers (inset Figure 10). In this region, the transport can be described by phonon assisted tunnelling of electrons between localised states, so that ρ, is defined as $\rho = \rho_0 \exp(T_0/T)^{0.25}$. The localisation temperature, T_0 = 2.1 x 10^6 K ($T_0 = \lambda\alpha^3/k_B N(E_F)$), where T_0 reflects the degree of electronic disorder, λ is a dimensionless constant, α^{-1} is equal to the localisation length and $N(E_F)$ is the density of localised states at E_F. A localisation temperature of this magnitude indicates a heavily electronically disordered system so that the hopping length is long, and the resistivity increases rapidly upon cooling and becomes immeasurable below 210 K. Similar electronic behaviour is exhibited in cobalt doped $NdMnAsO_{0.95}F_{0.05}$ phases [30]. $Sr_2Mn_3As_2O_2$ contains semiconducting $Mn_2As_2^{2-}$ layers [14, 15, 16 17]. In contrast $Sr_2Cr_3As_2O_2$ is metallic [11], with the metallic conduction predominantly arising from the $Cr_2As_2^{2-}$ layers [11]. $Sr_2Mn_{2.23}Cr_{0.77}As_2O_2$ contains $Mn_{1.92}Cr_{0.08}As_2^{2-}$ layers and hence is semiconducting. Mn pnictides tend to be semiconducting due to the stronger hybridisation between Mn 3*d* and pnictogen *p* states.

CONCLUSIONS

In summary, analogously to the 1111 Mn oxypnictides, $Sr_2Mn_{2.23}Cr_{0.77}As_2O_2$ exhibits multiple magnetic transitions and it would appear that there is magnetic coupling between the MO_2^{2-}planes and the $M'_2As_2^{2-}$ slabs which gets stronger as the Cr concentration increases from x = 0 - 3. Variable pressure neutron diffraction studies of $Sr_2M_3As_2O_2$ phases would be interesting to further investigate the superexchange interactions as a function of unit cell size.

Similar to the 1111 Mn oxypnictides, $Sr_2Mn_{2.23}Cr_{0.77}As_2O_2$ is semiconducting. However, the resistivity is too high to measure below 210 K and so it is not possible to ascertain whether there is any magnetoresistance as the Mn/Cr moments within the arsenide layers flip from a G-type to a C-

type antiferromagnetic arrangement. Electron doping of the $M'_2As_2^{2-}$ slabs is warranted to investigate this further.

ASSOCIATED CONTENT

Supporting Information. The supporting information includes Rietveld fits from neutron diffraction and synchrotron X-ray diffraction data and tables of crystallographic data.

AUTHOR INFORMATION

Corresponding Author

*a.c.mclaughlin@abdn.ac.uk

Tel: 0044 1224272924; Fax: 0044 1224272921

Author Contributions

The manuscript was written through contributions of all authors. All authors have given approval to the final version of the manuscript.

ACKNOWLEDGMENT

This research is supported by the EPSRC (research grant EP/L002493/1). We also acknowledge the UK Science and Technology Facilities Council (STFC) for provision of beam time at the ILL.

REFERENCES

(1) Kamihara, Y.; Watanabe, T.; Hirano, M.; Hosono, H. Iron-based layered superconductor La[$O_{1-x}F_x$]FeAs (x = 0.05−0.12) with T_c = 26 K. *J. Amer. Chem. Soc*. **2008**, *130*, 3296-3297.

(2) Wildman, E. J.; Skakle, J. M. S.; Emery, N.; Mclaughlin, A. C. Colossal magnetoresistance in Mn^{2+} oxypnictides $NdMnAsO_{1-x}F_x$. *J. Amer. Chem. Soc*. **2012**, *134*, 8766-8769.

(3) Rotter, M.; Tegel, M.; Johrendt, D. Superconductivity at 38 K in the iron arsenide ($Ba_{1-x}K_x$)Fe_2As_2. *Phys. Rev. Lett*. **2008,** *101*, 107006.

(4) Zhu, X.; Han, F.; Mu, G.; Cheng, P.; Shen, B.; Zeng, B.; Wen, H-H. Transition of stoichiometric Sr_2VO_3FeAs to a superconducting state at 37.2 K. *Phys. Rev. B*. **2009**, *79*, 220512.

(5) Paglione, J.; Greene, R. L. High-temperature superconductivity in iron-based materials. *Nat. Phys*. **2010**, *6*, 645-658.

(6) Wildman, E. J.; Mclaughlin, A. C. A variable temperature synchrotron x-ray diffraction study of colossal magnetoresistant $NdMnAsO_{0.95}F_{0.05}$. *Sci. Rep*. **2016**, *6*, 20705.

(7) Wildman, E. J.; Sher, F.; Mclaughlin, A. C.; Absence of colossal magnetoresistance in the oxypnictide $PrMnAsO_{0.95}F_{0.05}$. *Inorg. Chem*. **2015**, *54*, 2536-2542.

(8) Emery, N.; Wildman, E. J; Skakle, J. M. S.; Mclaughlin, A. C.; Smith, R. I.; Fitch, A. N. Variable temperature study of the crystal and magnetic structures of the giant magnetoresistant materials *L*MnAsO (*L* = La, Nd). *Phys. Rev. B.* **2011**, *83*, 144429.

(9) Nath, R.; Garlea, V. O.; Goldman, A. I.; Johnston, D. C. Synthesis, structure, and properties of tetragonal $Sr_2M_3As_2O_2$ (M_3=Mn_3, Mn_2Cu, and $MnZn_2$) compounds containing alternating CuO_2-type and FeAs-type layers. *Phys. Rev. B.* **2010,** *81*, 224513.

(10) Ozawa, T.; Olmstead, M. M.; Brock, S. L.; Kauzlarich, S. M.; Young, D. M. Synthesis and Characterization of a new compound with alternating MnO_2^{2-} and $Zn_2As_2^{2-}$ layers: $Ba_2MnZn_2As_2O_2$. *Chem. Mater*. **1998**, *10*, 392-396.

(11) Jiang, H.; Bao, J.-K.; Zhai, H.-F.; Tang, Z.-T.; Sun, Y.-L.; Liu, Y.; Wang, Z.-C.; Bai, H.; Xu, Z.-A.; Cao, G.-H. Physical properties and electronic structure of $Sr_2Cr_3As_2O_2$ containing CrO_2 and Cr_2As_2 square-planar lattices. *Phys. Rev. B.* **2015**, *92*, 205107.

(12) Liu, J.; Wang, J.; Sheng, J.; Ye, F.; Taddei, K.; Fernandez-Baca, J.; Luo, W.; Sun, G.; Wang, Z.; Jiang, H.; Cao, G.; Bao, W. Neutron diffraction study on magnetic structures and transitions in $Sr_2Cr_3As_2O_2$. *Phys. Rev. B.* **2018**, *98*, 134416.

(13) Brechtel, E.; Cordier, G.; Schaefer, H. Über oxidpnictide: zur kenntnis von $A_2Mn_3B_2O_2$ mit A = Sr, Ba und B = As, Sb, Bi. *Z. Naturforsch. B.* **1979**, *34*, 777-780.

(14) Brock, S. L.; Kauzlarich, S. M. Structure-property relationships in a series of mixed layer pnictide oxide compounds: $A_2Mn_3Pn_2O_2$ (A= Sr, Ba; Pn=P, As, Sb). *J. Alloys Compd.* **1996**, *241*, 82-88.

(15) Brock, S. L.; Raju, N. P.; Greedan, J. E.; Kauzlarich, S. M. The magnetic structures of the mixed layer pnictide oxide compounds $Sr_2Mn_3Pn_2O_2$ (Pn = As, Sb). *J. Alloys Compd.* **1996**, *237*, 9-19.

(16) Singh, Y.; Green, M. A.; Huang, Q.; Kreyssig, A.; McQueeney, R. J.; Johnston, D. C.; Goldman, A. I. Magnetic order in $BaMn_2As_2$ from neutron diffraction measurements. *Phys. Rev. B.* **2009**, *80*, 100403.

(17) Ozawa, T.; Kauzlarich, S. M.; Bieringer, M.; Wiebe, C. R.; Greedan, J. E.; Gardner, J. S. The effect of interlayer cations on the magnetic properties of the mixed-metal pnictide oxides: $A_2MnZn_2As_2O_2$ (A = Sr, Ba). *Chem. Mater.* **2001**, *13*, 973-980.

(18) Singh, D. J.; Sefat, A. S.; McGuire, M. A.; Sales, B. C.; Mandrus, D.; VanBebber, L. H.; Keppens, V. Itinerant antiferromagnetism in $BaCr_2As_2$: Experimental characterization and electronic structure calculations *Phys. Rev. B.* **2009**, *79*, 094429.

(19) Park, S.-W.; Mizoguchi, H.; Kodama, K.; Shamoto, S.-I.; Otomo, T.; Matsuishi, S.; Kamiya, T.; Hosono, H. Magnetic structure and electromagnetic properties of LnCrAsO with a ZrCuSiAs-type structure (Ln = La, Ce, Pr, and Nd). *Inorg. Chem*. **2013**, *52,* 13363-13368.

(20) Fauth, F.; Boer, R.; Gil-Ortiz, F.; Popescu, C.; Vallcorba, O.; Peral, I.; Fulla, D.; Benach, J.; Juanhuix, J. The crystallography stations at the ALBA synchrotron. *Eur. Phys. J. Plus.* **2015**, *130*, 160.

(21) Van der Linden, P. J. E. M.; Moretti Sala, M.; Henriquet, C.; Rossi, M.; Ohgushi, K.; Fauth, F.; Simonelli, L.; Marini, C.; Fraga, E.; Murray, C.; Potter, J.; Krisch, M. A Compact And Versatile Dynamic Flow Cryostat For Photon Science. *Rev. Sci. Instrum.* **2016**, *87* (11), 115103.

(22) Rietveld, H. A profile refinement method for nuclear and magnetic structures. *J. Appl. Crystallogr*. **1969**, *2*, 65-71.

(23) Rodríguez-Carvajal, J. Recent advances in magnetic structure determination by neutron powder diffraction. *Physica B.* **1993**, *192*, 55-69.

(24) Waroquiers, D.; Gonze, X.; Rignanese, G.; Welker-Nieuwoudt, C.; Rosowski, F., Göbel, M.; Schenk, S.; Degelmann, P.; André R.; Glaum, R.; Hautier, G. Statistical analysis of coordination environments in oxides. *Chem. Mater.* **2017**, *29*, 8346-8360.

(25) Vaknin, D.; Sinha, S.; Moncton, D.; Johnston, D.; Newsam, J.; Safinya, C.; King, H. Antiferromagnetism in La_2CuO_{4-y}. *Phys. Rev. Lett.* **1987**, *58*, 2802-2805.

(26) Dagotto, E.; Hotta, T.; Moreo, A. Colossal magnetoresistant materials: The key role of phase separation. *Phys. Rep.* **2001**, *344*, 1–153.

(27) Peng, J., Liu, J., Hu, J., Mao, Z., Zhang, F. and Wu, X. Magnetic phase separation in double layer ruthenates $Ca_3(Ru_{1-x}Ti_x)_2O_7$. *Sci. Rep.* **2016**, *6*, 19462.

(28) Hong, K. H.; Arevalo-Lopez, A. M.; Cumby, J. Ritter, C.; Attfield, J. P. Long range electronic phase separation in $CaFe_3O_5$. *Nat. Commun*. **2018**, *9*, 2975.

(29) Park, J. T. et al. Electronic phase separation in the slightly underdoped iron pnictide superconductor $Ba_{1-x}KxFe_2As_2$. *Phys. Rev. Lett.* **2009**, *102*, 117006.

(30) Wildman, E. J.; McCombie, K. S.; Stenning, G. B. G.; Mclaughlin, A. C. The suppression of CMR in $NdMn_{1-x}Co_xAsO_{0.95}F_{0.05}$. *Dalton. Trans.* **2018**, *47*, 14726-14733.